RSC Advances

PAPER

View Article Online
View Journal | View Issue

Cite this: *RSC Adv.*, 2023, **13**, 11959

Dimethyl sulfoxide as a function additive on halogen-free electrolyte for magnesium battery application

R. Gamal,[a] E. Sheha *[b] and M. M. El Kholy*[cd]

Practical Mg batteries still face significant challenges in their development, like the lack of simple compatible electrolytes, self-discharge, the rapid passivation of the Mg anode, and the slow conversion reaction pathway. Here, we propose a simple halogen-free electrolyte (HFE) based on magnesium nitrate ($Mg(NO_3)_2$), magnesium triflate $Mg(CF_3SO_3)_2$, and succinonitrile (SN) dissolved in acetonitrile (ACN)/tetraethylene glycol dimethyl ether (G4) cosolvents, with dimethyl sulfoxide as a functional additive. The addition of DMSO to the HFE changes the interfacial structure at the magnesium anode surface and facilitates the transport of magnesium ions. The as-prepared electrolyte shows high conductivity (σ_b = 4.48 × 10^{-5}, 6.52 × 10^{-5} and 9.41 × 10^{-5} S cm^{-1} at 303, 323, and 343 K, respectively) and a high ionic transference number ($t_{mg^{+2}}$ = 0.91/0.94 at room temperature/55 °C) for the matrix containing 0.75 ml of DMSO. Also, the cell with 0.75 ml of DMSO shows high oxidation stability, a very low overpotential, and steady Mg stripping/plating up to 100 h. Postmortem analysis of pristine Mg and Mg anodes extracted from disassembled Mg/HFE/Mg and Mg/HFE_0.75 ml DMSO/Mg cells after stripping/plating reveals the role of DMSO in improving Mg-ion passage through HFE by evolving the anode/electrolyte interface at the Mg surface. Further optimization of this electrolyte is expected to achieve excellent performance and good cycle stability when applied to the magnesium battery in future work.

Received 15th March 2023
Accepted 12th April 2023

DOI: 10.1039/d3ra01707a

rsc.li/rsc-advances

Introduction

Magnesium batteries have recently become promising post-lithium batteries due to their low reduction potential, earthly abundance, safety, and high theoretical capacity (3837 A h L^{-1}). Nonetheless, the low reduction potential of Mg rapidly decreases the electrolyte species forming a passivation layer on the Mg/electrolyte interface with high Mg^{2+} transfer impedance, which hinders reversible Mg stripping/plating.[1,2] Innovative approaches to develop electrolytes without passivation for the Mg anode and facilitating the transport of Mg-ions have become an important demand for producing practical magnesium batteries. A few examples of electrolytes have been studied for reversible Mg deposition/stripping achieving high anodic stability (~4.0 V *vs.* Mg), such as Magnesium carba-*closo*-decaborate ($Mg(HCB_{11}H_{11})_2$),[3] magnesium aluminum hexafluoroisopropoxide ($Mg[Al\text{-}(HFIP)_4]_2$),[4] magnesium tetrakis(hexafluoroisopropyloxy)borate ($Mg[B(HFIP)_4]_2$),[5] and magnesium hexamethyldisilazane ($Mg(HMDS)_2$).[6] However, $Mg(HCB_{11}H_{11})_2$ is very expensive and limited in commercial applications. Both $Mg[B(HFIP)_4]_2$ and $Mg[Al\text{-}(HFIP)_4]_2$ lack chemical stability under ambient conditions where they decompose chemically in the presence of moisture.[4] Low plating/stripping efficiency and poor short-term cycling performance limit the use of $Mg(HMDS)_2$ electrolyte, which requires the addition of either $MgCl_2$ or $AlCl_3$.[7,8] The introduction of Cl^- and Al-containing Lewis acids ($AlCl_3$, $AlEtCl_2$, and Me_2AlCl) has been considerably employed to increase the anodic stability and anode electrolyte interface compatibility and also dissolve passivating species on the surface of the Mg anode, which enhances reversible Mg plating/stripping, but its existence may cause critical corrosion of the common current collectors like SS, Al, and Cu.[9] This corrosion has an opposite impact on the long-term cycle of magnesium batteries and eventually makes the batteries invalid.[9,10]

Dimethyl sulfoxide ($(CH_3)_2SO$, designated DMSO) is known as "green solvent" (organosulfur) for inorganic/organic materials having a low melting point (19 °C), high boiling point (189 °C), high dielectric permittivity (dielectric constant, ε = 46.7), high electrochemical stability, high resistance to redox reactions, good miscibility with water, low toxicity, and is a highly polar aprotic solvent because of its S=O group.[5,11–14] The high polarity of DMSO is caused by two reasons: first, the highly polar nature of DMSO molecules, and second, the unusual geometrical structure of DMSO molecules significantly reduces their

[a]*Physics Department, Belbeis High Institute of Engineering (BHIE), Belbeis, Sharqia*
[b]*Physics Department, Faculty of Science, Benha University, Benha, 13518, Egypt. E-mail: islam.shihah@fsc.bu.edu.eg*
[c]*Physics Department, Faculty of Science, Menoufia University, Shibin El-Kom, Egypt. E-mail: president@nmu.edu.eg*
[d]*Physics Department, Faculty of Science, New Mansoura University, Dakahlia, Egypt*

ability to form antiparallel dipolar aggregations,[5] so it is a suitable medium for utilization in high-energy batteries[15,16] and double-layer capacitors[17,18] in both pure form and in combinations with other liquids. Kheawhom *et al.* studied the effect of DMSO in KOH aqueous electrolytes on the performance of a zinc–air flow battery, revealing a critical role for DMSO in the dissolution and deposition of zinc. The introduction of DMSO improved zinc dissolution performance, decreased polarization resistance, moreover, improved the discharge capacity, and demonstrated excellent cyclability.[12] Kheawhom *et al.* investigated the application of a DMSO-based electrolyte in zinc-ion batteries (ZIBs), using a MnO_2 cathode. The reversibility of Zn stripping/plating in DMSO-based electrolytes is good, and also, the battery delivers a high specific capacity, and the retention is recorded 60% after 1000 cycles.[19] Cheng *et al.* studied the possibility of replacing *N*-methylprrolidone (NMP) with DMSO (a low-toxicity solvent) to dissolve poly vinylidene fluoride (PVDF) to reduce the environmental hazards and cost of lithium-ion battery (LIBs) manufacturing. The viscosity and electrochemical measurements results, scanning electron microscopy (SEM), and X-ray photoelectron spectroscopy (XPS) show that DMSO can replace the NMP without altering the conventional LIB manufacturing process.[20]

Developing halogen-free electrolytes (HFE) is a turning point in studying and developing magnesium electrolytes.[21,22] HFE is very compatible with Mg metal, where observed great oxidative stability that of ether solvents, due to its inertness and non-corrosive nature.[21] Therefore, the development of HFE from low-cost, commercially available chemicals is very wanted to deliver high electrochemical performance and chemical stability simultaneously. Magnesium triflate is a promising salt for high-voltage electrolyte systems, non-toxic, and insensitive to moisture. An early study reported reversible stripping/plating of magnesium from electrolyte system-based magnesium triflate. However, the low solubility in ethereal solvents and metal passivation due to modulation of the solubility with ionic liquid is still a drawback for realizing an efficient electrolyte-based magnesium triflate.[23] The as-prepared Mg-ion electrolyte-based ($Mg(NO_3)_2\cdot 6H_2O$) exhibits efficient Mg plating/stripping performance. The chronoamperometry plating profile at Pt electrode displayed nondendritic, flat, and translucent crystals of the Mg element.[24] The challenge of low solubility and incompatibility can be bypassed by integrating $Mg(CF_3SO_3)_2$ with ($Mg(NO_3)_2\cdot 6H_2O$) in a cosolvent solution to realize an efficient electrolyte. Recently, a simple halogen-free electrolyte-based $Mg(NO_3)_2\cdot 6H_2O$ $Mg(CF_3SO_3)_2$, SN dissolved in ACN/G4 has been investigated and tested in an Mg/S battery. However, this electrolyte exhibited promising results;[25] future work must focus on overcoming the low coulombic efficiency and the short cycle life. Recently, a simple halogen free electrolyte based $Mg(NO_3)_2\cdot 6H_2O$ dissolved in ACN/G4 has been investigated and tested in an Mg/S battery, though this electrolyte exhibited non-dendritic, and high initial discharge capacity;[26] future work must be focused on trying to overcome the low coulombic efficiency and the short cycle life. Introducing DMSO into HFE may enhance the dissolution of salts owing to its high polarity and enhance the mobility of Mg-ions, which evolve at the anode/electrolyte interface; as a result, charge transfers will increase.

In light of the above concerns, we submitted a reaction scheme that involved active species of $Mg(NO_3)_2\cdot 6H_2O$, $Mg(CF_3SO_3)_2$, SN, and the variable ratio of DMSO in ACN : G4($\sim$2 : 1); HFE_DMSO. The effect of DMSO on the structural, optical, electrical, and electrochemical properties of the HFE has been investigated. The X-ray diffraction (XRD), energy-dispersive X-ray spectroscopy (EDS), scanning electron microscopy (SEM), and transform infrared (FTIR) techniques are studied to identify the structure evolution of pristine Mg and Mg anode extracted from disassembled Mg/HFE/Mg and Mg/HFE_0.75 ml DMSO/Mg cells after stripping/plating.

Experimental technique

HFE based 1.1 g of $Mg(NO_3)_2\cdot 6H_2O$ salt (pre-calcined at 80 °C), 0.4 g of $Mg(CF_3SO_3)_2$ (Alfa Aesar) and 0.03 g SN dissolved in 5.4/2.7 ml of ACN/G4 was synthesized according to our previous research.[25] HFE_DMSO was prepared by adding different DMSO concentrations (Loba Chemie) (x = 0, 0.25, 0.5, 0.75, 1 ml) to 5 ml of HFE and stirred for 24 h. HFE_DMSO will be denoted by HFE_0 (x = 0 ml), HFE_1 (x = 0.25 ml), HFE_2 (x = 0.5 ml), HFE_3 (x = 0.75 ml) and HFE_4 (x = 1 ml). XRD patterns were obtained through X-ray Diffractometer (Rigaku MiniFlex 600) with line focus Cu Kα radiation ($\lambda \approx 1.542$ Å), and SEM was performed by the JEOL JSM-7000 attached to the EDS unit. FTIR was recorded from the Alpha II FT-IR spectrometer. A DS5 Dual Beam UV-Vis Spectrophotometer recorded the optical absorptions. Electrochemical impedance spectroscopy (EIS) at various temperatures (303–348 K) and frequencies (10 to 10^6 Hz) was measured using the CHI604E electrochemical workstation in a SS/HFE_DMSO/SS electrolytic coin cell (CR2032), which was assembled in an Ar-filled glove box. The optimum sample (HFE_3) was used to investigate the electrochemical stability of HFE_DMSO at room temperature (RT) and 55 °C, and was measured using a two-electrode coin cell with stainless steel as a working electrode and Mg foil as both the reference and counter electrodes. The magnesium-ion transference number of the Mg/Mg cell was measured by AC impedance before (B) and after (A) polarization and direct-current (DC) polarization (with a DC voltage of 0.1 volts) at RT and 55 °C. The stripping/plating (SP) of symmetric Mg/Mg cell were performed on a NEWARE BTS4000 tester over 100 h. The XRD, EDS, SEM, and FTIR analyses of pristine Mg and Mg anodes extracted from disassembled Mg/HFE_0/Mg and Mg/HFE_3/Mg cells after stripping/plating have been investigated.

Results and discussion

The interplay between the functional groups of HFE_0 and DMSO was characterized using FTIR spectroscopy. Fig. 1a and b shows FTIR spectra for SN, DMSO, HFE_0, HFE_1, HFE_2, HFE_3, and HFE_4 in the wavenumber ranges of 400–2000 and 2000–4000 cm^{-1}, respectively. The bands located at 3404, 2890, 1660, 1330, 1091, 1027 cm^{-1} and 2250 cm^{-1} were assigned to O–H stretching, C–H stretching, C=O stretching, C–H bending, C–O–C

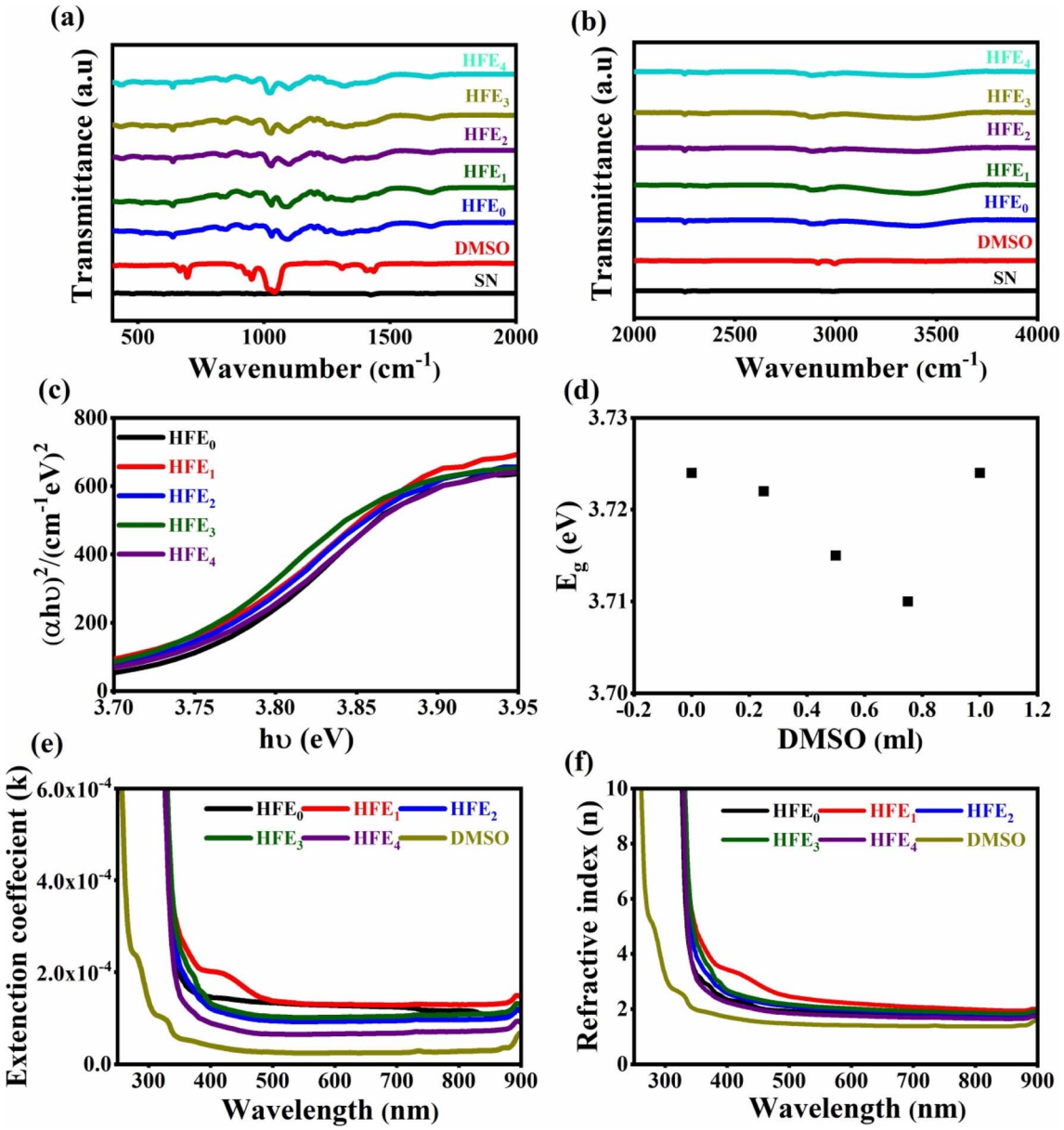

Fig. 1 FTIR spectra in the wavenumber range of (a) 400–2000 cm^{-1}, (b) 2000–4000 cm^{-1}; UV–visible spectra (c) Tauc plot, (d) variation of energy band gap as a function of DMSO content, (e) extinction coefficients (k), (f) refractive index (n), for HFE_DMSO.

stretching, S=O stretching and –CN stretching vibration of HFE_0.[25] The introduction of DMSO within the framework of HFE_0 perturbed the bonding scheme of HFE_0, causing reduction in the intensity of the peaks and small redshifts, which confirm the complexation between DMSO and HFE.[27–32] UV-spectroscopy is an effective method for investigating changes in electronic energy levels inside a molecule produced by electron transfer from π- or non-bonding orbitals. Fig. 1c–f shows the UV–vis spectra of HFE_DMSO. The optical band gap is an essential parameter for characterizing electronic electrolyte transitions. The optical bandgap energies (E_g) can be calculated using the Tauc equation:[33,34]

$$\alpha h\nu = B(h\nu - E_g)^n \quad (1)$$

α is the absorption coefficient, $h\nu$ is the incident photon energy, and B is the constant. E_g values are calculated by scheming $(\alpha h\nu)^2$ *versus* $h\nu$ (Fig. 1c) and can be calculated by extrapolating the linear portion of the curve to the x-axis.

Fig. 1d illustrates the E_g values *versus* the content of DMSO. The lowest band gap was observed at HFE_3, where the band gap began to widen, which matches the Burstein Moss effect.[35] The introduction of DMSO after a certain amount changed the ratio of the solute to the solvent and reduced the density of the state.[36] The extinction coefficient (k) and the refractive index (n) are essential parameters for characterizing the optical properties of electrolytes and can be obtained using the following equations:[33,34]

$$\alpha = \frac{2.303\ A}{d} \quad (2)$$

A is the absorbance, and d is the thickness of the sample.

$$K = \frac{\alpha\lambda}{4\pi} \quad (3)$$

λ is wavelength

$$n = \frac{(1+R)}{(1-R)} + \sqrt{\frac{4R}{(1-R)^2} - K^2} \quad (4)$$

R denotes reflectance. Fig. 1e and f shows the relation between the extinction coefficient and refractive index with the incident light wavelengths (λ) for HFE_DMSO, respectively. The extinction coefficient decreased with increasing the wavelength and with the introduction of DMSO, and the refractive index decreased with increasing the wavelength and increased with the introduction of DMSO, which reflects that the addition of DMSO affects the velocity of electromagnetic waves within the HFE medium. Fig. 2a and b shows the Cole–Cole plot for HFE_DMSO. The plots illustrate semicircle diameter (which represents the bulk resistance R_b) decreases with increasing the concentration of DMSO, and the sample HFE_3 shows the lowest resistance. The ionic conductivity can be calculated from the relation:[37]

$$\sigma_b = \frac{1}{R_b} \times \frac{t}{A} \quad (5)$$

where t and A are the electrolyte's thickness and active surface area, respectively, Fig. 2c illustrates the ionic conductivity of HFE_DMSO as a function of DMSO concentrations at 303, 323, and 343 K. The conductivity increased with increasing DMSO concentration and temperature, reaching 4.48×10^{-5}, 6.52×10^{-5} and 9.41×10^{-5} S cm^{-1} at 303, 323, and 343 K, respectively, which could be attributed to DMSO's high polarity and permittivity, *i.e.*, its ability to act as a solvent for Mg salt and the gradual dissociation of the ion pairs in the HFE-producing charge carriers while also decreasing viscosity. The conductivity gradually decreases after the optimal concentration. This decrease may be explained according to equation:[38]

$$\sigma = nq\mu \quad (6)$$

where n, q, μ is the number of charge carriers, the charge of the carrier density, and the mobility of the carriers, respectively. Increasing the DMSO ratio after a certain amount (0.75 ml) decreases the solute to the solvent, reducing charge carriers' concentration. Therefore, the ionic conductivity decreased with increasing DMSO after this amount. Fig. 2d shows the relation

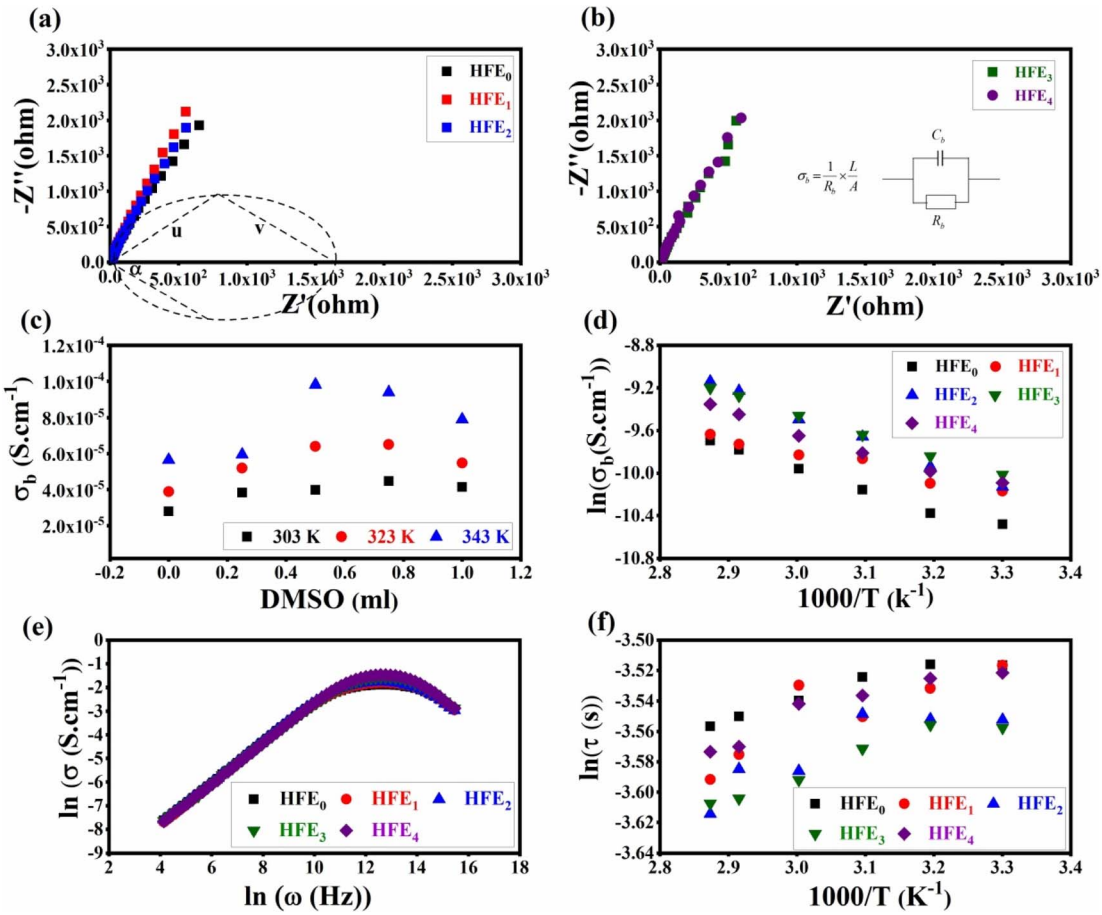

Fig. 2 (a and b) Col–col plots, (c) variation of bulk conductivity with DMSO content, (d) temperature dependent of bulk conductivity, (e) temperature dependent of frequency (ω), (f) temperature dependent of relaxation time (τ), for HFE_DMSO.

between temperature and ionic conductivities for HFE_DMSO from 303 to 348 K. The behavior obeys the Arrhenius relation:[39]

$$\sigma = \sigma_o \, e^{\left(-\frac{E_a}{KT}\right)} \quad (7)$$

where σ_o, E_a, K_B, and T are the pre-exponential factor, the activation energy of ion conduction, the Boltzmann constant, and the temperature in Kelvin, respectively. The conductivity increases with increasing temperature, following the Arrhenius law. From the linear fitting of $\ln \sigma \sim 1/T$, the activation energies have been calculated and listed in Table 1. The table shows that at the first region (3.3 to 3.1 K^{-1}), the lowest activation energy is for HFE_3. Fig. 2d shows the conductivity of HFE_DMSO as a function of frequency at 303 K. The conductivity of samples increases with frequency. At low frequencies, charges accumulate close to the electrodes and electrode interfaces, which decreases the quantity of free mobile ions and reduces conductivity. The conductivity increases with frequency at higher frequencies because of the quicker hopping of ions.[11,40] The general behavior obeys the universal power law:[11]

$$\sigma_{tot}(\omega) = \sigma_{dc} + A\omega^s \quad (8)$$

where σ_{dc} is the dc conductivity, A is the pre-exponential factor, ω is the angular frequency of the applied electric field, and s is the exponent factor. The values of the exponent factor can be calculated by using the least square fitting of the last equation. The values of s lie within the range of $0.79 \leq s \leq 0.82$, so the conduction occurs by the hopping conduction mechanism.[11,41]

The relaxation time (τ) can be calculated from the relation:[37]

$$\frac{\nu}{\upsilon} = (\omega\tau)^{1-h} \quad (9)$$

where ν is the distance on the impedance plot between (O, R_b) and an experimental point, υ is the distance between the experimental point and (0, 0), ω is the angular frequency, and $h = \frac{2\alpha}{\pi}$ where α is the depressed angle from the Z'-axis (Fig. 2a). Fig. 2f shows the relation between temperature and relaxation time (τ) for HFE_DMSO. The relaxation time decreases with increasing the temperature and concentration of DMSO, and the behavior obeys the Arrhenius relation.

$$\tau = \tau_o e^{\left(\pm \frac{\Delta E_r}{KT}\right)} \quad (10)$$

Table 1 Electrical and diffusion parameters of HFE_DMSO

HFE_0		HFE_1	HFE_2	HFE_3	HFE_4	
σ (S cm^{-1}) (RT)		2.80 × 10^{-5}	3.83 × 10^{-5}	3.99 × 10^{-5}	4.48 × 10^{-5}	4.15 × 10^{-5}
E_aI (eV)		2.12	2.08	1.76	1.59	2.17
E_aII (eV)		0.99	1.39	1.09	1.02	1.51
$E_\tau I$ (eV)		0.06	0.16	0.02	0.04	0.07
$E_\tau II$ (eV)		0.16	0.21	0.18	0.12	0.23
$t_{mg^{+2}}$	RT	0.8			0.91	
	55 °C	0.9			0.94	

where τ_o is a quantity that is the inverse of the oscillation frequency of the dipole in its potential well, and ΔE_r is the activation energy of relaxation. The decrease in the relaxation time values with increasing temperature could be attributed to dipole freedom.[26] The activation energy of relaxation has been calculated using the last equation's least square fitting and is listed in Table 1. According to the timely results, introducing dimethyl sulfoxide (DMSO) within the skeleton of HFE causes redesigning the solvation shell surrounding each Mg^{2+} ion, which reduces the solvation barrier of Mg^{2+} ions so does reduce the viscosity and increasing the ionic conductivity of the electrolyte solution.[42,43] The above findings confirm that sample HFE_3 as the optimum sample, so it was chosen as the main sample for subsequent experiments. The value of the Mg^{+2} ion transference number ($t_{mg^{+2}}$) is very important in determining the performance and rate capability of the electrolyte for battery applications. The magnesium ion transference number $t_{mg^{+2}}$ was obtained by using the equation:[37]

$$t_{mg^{+2}} = \frac{I_s(\Delta V - I_o R_o)}{I_o(\Delta V - I_s R_s)} \quad (11)$$

where I_0 and I_s are the initial and final currents, R_0 and R_s are the cell resistances before (B) and after (A) polarization, respectively, and ΔV is the DC voltage applied to polarize the sample. The impedance spectra before and after polarization and the variation of the polarization current as a function of time are shown in Fig. 3a and b for $Mg/HFE_0/Mg$ and $Mg/HFE_3/Mg$ cells at RT and 55 °C, respectively. It is noticed that the introduction of DMSO increased the sample's current at RT and 55 °C and the current dropped with time until it reached a steady state. The value of $t_{mg^{+2}}$ increased with the addition of DMSO, reaching 0.91/0.94 at RT/55 °C. Linear sweep voltammetry (LSV) was used to study the effect of DMSO on the oxidation stability of HFE by using a SS/Mg coin cell. Fig. 3c shows the LSV of $SS/HFE_0/Mg$ and $SS/HFE_3/Mg$ coin cells with a voltage range from −1 to 5 V at RT/55 °C. Fig. 3c shows that HFE_3 electrolyte with the addition of DMSO displays a high current increase and oxidation stability up to 4.8/3.7 V at RT/55 °C, which confirms the high electrochemical stability window of HFE_3. To investigate the electrochemical stability of HFE_3, the reversibility of Mg plating/stripping processes was studied at RT/55 °C. Fig. 3d illustrates the stripping platting (SP) curves of $Mg/HFE_0/Mg$ and $Mg/HFE_3/Mg$ with a current density of 0.02 mA cm^{-2} at RT/55 °C. The addition of DMSO significantly improved electrolyte stability with a relatively low overpotential up to 100 h, indicating the role of DMSO in improving Mg-ion passage through HFE by evolving the anode/electrolyte interface at the Mg surface.[44] The reduction in the stripping/plating potential amplitude of $Mg|HFE_3|Mg$ at 55 °C after 65 hours confirms that the electrolyte is under an electrochemical conditioning step which cleans them from active contaminants.[45] SEM micrographs of pristine Mg and Mg anode extracted from disassembled $Mg/HFE_0/Mg$ (Mg_HFE_o) and $Mg/HFE_3/Mg$ (Mg_HFE_3) cells after stripping/plating are shown in Fig. 3e–g. The surface of pristine Mg shows flat and uniform morphology, while the Mg_HFE_o surface shows stick morphology. After the introduction of DMSO (Mg_HFE_3) the

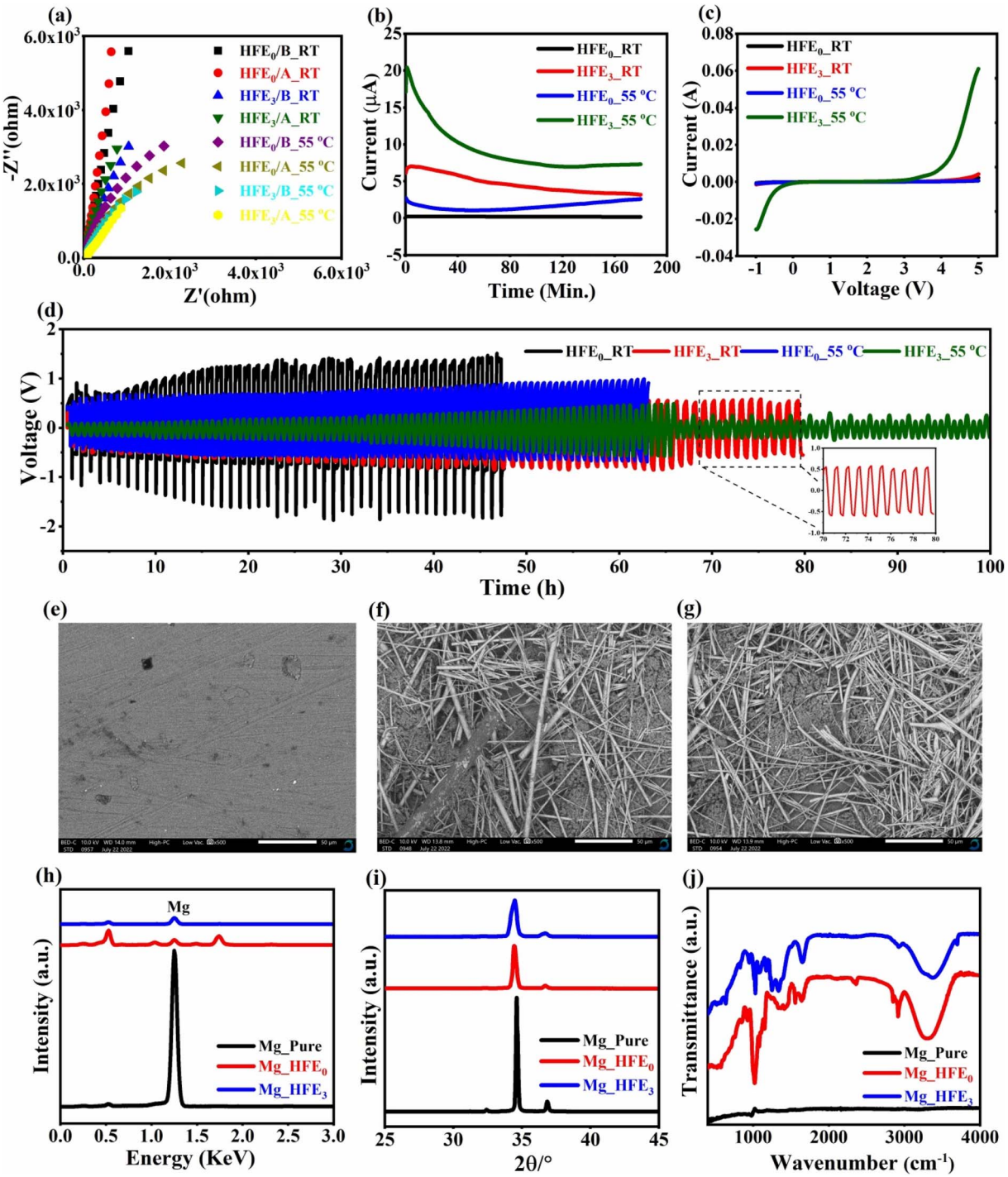

Fig. 3 a Nyquist plots before and after DC polarization, (b) DC polarization curve for Mg/HFE_0/Mg and Mg/HFE_3/Mg cells; (c) linear sweep voltammetry (LSV) for SS/HFE_0/Mg and SS/HFE_3/Mg cells; (d) Mg stripping/plating (SP) for symmetric Mg/HFE_0/Mg and Mg/HFE_3/Mg cells; SEM micrographs (insets: amplified voltage profiles) (e) pristine Mg, (f) Mg_HFE_o, (g) Mg_HFE_3; (h) EDS, (i) XRD, (j) FTIR spectra for Mg, Mg_HFE_o and Mg_HFE_3.

density of sticks increased, which may be related to the role of DMSO in enhancing the mobility of Mg-ions through the electrolyte, as mentioned above. The EDS spectra of Mg, Mg_HFE_o, and Mg_HFE_3 are shown in Fig. 3h. As shown, the reduction in the intensity of Mg's spectral line after stripping/plating is related to the evolution of the anode/electrolyte interface at the surface of the Mg-anode and the role of DMSO in changing its composition. XRD patterns of Mg, Mg_HFE_o, and Mg_HFE_3 are shown in Fig. 3i, and the results match the hexagonal Mg (JCPDS No. 901-3058). The pattern illustrates slight shifts and a reduction in the intensity of the peaks related to the evolution of the interface at the Mg surface, as mentioned above. The

FTIR spectra of Mg, Mg_HFE$_o$, and Mg_HFE$_3$ are shown in Fig. 3j; the results illustrated the spectral characteristics of Mg_HFE$_o$ and Mg_HFE$_3$ consistent with HFE[25] lines ($\sim$1089 cm^{-1}, $\sim$1648–1650 cm^{-1}, and $\sim$2898–2902 cm^{-1} match the stretching vibration of C–O, C=C, and C–H, respectively). The intensity of Mg_HFE$_3$ was reduced compared with Mg_HFE$_o$ and accompanied by a slight shift in wave number, suggesting that DMSO altered the complexation of the anode/electrolyte interface and tailored its structure to a higher amorphous state.

Conclusion

In this study, we demonstrated the role of DMSO in optimizing the electrochemical performance of a halogen-free electrolyte (HFE) based on magnesium nitrate ($Mg(NO_3)_2$) and magnesium triflate $Mg(CF_3SO_3)_2$ dissolved in ACN/G4. The introduction of DMSO (HFE$_3$) resulted in very low overpotential and stable Mg stripping/plating, increasing the ionic conductivity values to $\sim 4.48 \times 10^{-5}$, 6.52×10^{-5} and 9.41×10^{-5} S. cm^{-1} at 303, 323, and 343 K, respectively, and increasing the ionic transference number to $t_{mg^{+2}} = 0.91/0.94$ at room temperature/55 °C. The XRD, EDS, SEM, and FTIR of pristine Mg and Mg anode extracted from disassembled Mg/HFE/Mg and Mg/HFE_0.75 ml DMSO/Mg cells after stripping/plating reveal the role of DMSO in improving Mg-ion passage through HFE by evolving the anode/electrolyte interface at the Mg surface. The outcomings emphasize the importance of this electrolyte system and it is expected to achieve excellent performance when applied in the magnesium battery in future work.

Conflicts of interest

There are no conflicts to declare.

Acknowledgements

This work is financially supported by Academy of Scientific Research Technology/Bibliotheca Alexandrina (ASRT/BA) (Grant No. 1530), ASRT (Grant No. 6631), STDF (Grant No. 30340).

References

1 M. F. H. S. R. E. Sheha, *J. Solid State Electrochem.*, 2022, **1**(1), 24.
2 X. Xu, C. Ye, D. Chao, B. Chen, H. Li, C. Tang, X. Zhong and S. Z. Qiao, *Adv. Mater.*, 2022, **34**, 2108688.
3 N. T. Hahn, T. J. Seguin, K.-C. Lau, C. Liao, B. J. Ingram, K. A. Persson and K. R. Zavadil, *J. Am. Chem. Soc.*, 2018, **140**, 11076–11084.
4 M. E. G. B. Zhirong Zhao-Karger, O. Fuhrbc and M. Fichtner, *J. Mater. Chem. A*, 2017, **5**, 10815–10820.
5 J. S. i. Iwona Płowas and N. Jan Jadzy, *J. Chem. Eng. Data*, 2014, **59**, 2360–2366.
6 C. Liao, N. Sa, B. Key, A. K. Burrell, L. Cheng, L. A. Curtiss, J. T. Vaughey, J.-J. Woo, L. Hu and B. Pan, *J. Mater. Chem. A*, 2015, **3**, 6082–6087.
7 Y. Y. Xinghe Zhao, Y. NuLi, D. Li, Y. Wang and X. Xiang, *Chem. Commun.*, 2019, **55**, 6086–6089.
8 X. Z. Zhirong Zhao-Karger, O. Fuhra and M. Fichtne, *RSC Adv.*, 2013, **3**, 16330–16335.
9 D. W. Wen Ren, Y. NuLi, X. Zhang, J. Yang and J. Wang, *ACS Appl. Mater. Interfaces*, 2021, **13**, 32957–32967.
10 X. Xu, D. Chao, B. Chen, P. Liang, H. Li, F. Xie, K. Davey and S. Z. Qiao, *Angew. Chem., Int. Ed.*, 2020, **59**, 21728–21735.
11 E. Sheha, *J. Adv. Res.*, 2015, **7**, 29–36.
12 A. A. Soraya Hosseini, L.-O. Uginet, N. Haustraete, S. Praserthdam, T. Yonezawa and S. Kheawhom, *Sci. Rep.*, 2019, **9**, 14958–14969.
13 R. B. Alvin Virya and K. Lian, *Electrochim. Acta*, 2021, **376**, 137984–137992.
14 A. B. Mahendra Nath Roy and R. K. Das, *J. Chem. Thermodyn.*, 2009, **41**, 1187–1192.
15 Z.-l. W. Dan Xu, Ji-j. Xu, L.-l. Zhang and X.-b. Zhang, *Chem. Commun.*, 2012, **48**, 6948–6950.
16 X. H. Bing Sun, S. Chen, J. Zhang and G. Wang, *RSC Adv.*, 2014, **4**, 11115–11120.
17 R. Kötza and M. Carlen, *Electrochim. Acta*, 2000, **45**, 2483–2498.
18 P. H. J. Partha Saha, M. K. Datta, C. U. Okoli, A. Manivannan and P. N. Kumta, *J. Electrochem. Soc.*, 2014, **161**, 593–598.
19 W. Kao-ian, M. T. Nguyen, T. Yonezawa, R. Pornprasertsuk, J. Qin, S. Siwamogsatham and S. Kheawhom, *Mater. Today Energy*, 2021, **21**, 100738.
20 X. D. Ming Wang, I. C. Escobar and Y.-T. Cheng, *ACS Sustainable Chem. Eng.*, 2020, **8**, 11046–11051.
21 R. M. Oscar Tutusaus, T. S. Arthur, F. Mizuno, E. G. Nelson and Y. V. Sevryugina, *Angew. Chem.*, 2015, **127**, 8011–8015.
22 J. Xiao, X. Zhang, H. Fan, Y. Zhao, Y. Su, H. Liu, X. Li, Y. Su, H. Yuan and T. Pan, *Adv. Mater.*, 2022, **34**, 2203783.
23 D.-T. Nguyen, A. Y. S. Eng, M.-F. Ng, V. Kumar, Z. Sofer, A. D. Handoko, G. S. Subramanian and Z. W. Seh, *Cell Rep. Phys. Sci.*, 2020, **1**, 100265.
24 E. Sheha, M. Farrag, S. Fan, E. Kamar and N. Sa, *ACS Appl. Energy Mater.*, 2022, **5**, 2260–2269.
25 R. Gamal, E. Sheha and M. M. El Kholy, *J. Electron. Mater.*, 2023, DOI: **10.1007/s11664-023-10364-3**.
26 M. F. Eslam Sheha, S. Fan, E. Kamar and N. Sa, *ACS Appl. Energy Mater.*, 2022, **5**, 2260–2269.
27 A. Pasha, A. S. Roy, M. V. Murugendrappa, O. A. Al-Hartomy and S. Khasim, *J. Mater. Sci.: Mater. Electron.*, 2016, **27**, 8332–8339.
28 S. A. Kirillov, M. I. Gorobets, M. M. Gafurov, K. S. Rabadanov and M. B. Ataev, *Russ. J. Phys. Chem. A*, 2014, **88**, 175–177.
29 B. B. Rahul Singh, S. K. Tomar, V. Singh and P. K. Singh, *Measurement*, 2017, **102**, 214–219.
30 O. Elkalashy and E. Sheha, *Appl. Phys. A: Mater. Sci. Process.*, 2018, **124**, 549.
31 N. Mansour, A. Momeni, R. Karimzadeh and M. Amini, *Opt. Mater. Express*, 2012, **2**, 740–748.
32 X. W. Huihui Wang, X. Zhang and C. Liu, *Molecules*, 2017, **22**, 1419–1430.
33 H. N. Abdelhamid, *Dalton Trans.*, 2023, **52**, 2506–2517.

34 B. Varshney, M. J. Siddiqui, A. H. Anwer, M. Zain Khan, F. Ahmed and H. A. Abdullah Aljaafari, *Sci. Rep.*, 2020, **10**, 11032–11045.
35 S. Li, G. Xie, D. V. Louzguine-Luzgin, Z. Cao, N. Yoshikawa, M. Sato and A. Inoue, *J. Alloys Compd.*, 2009, **476**, 482–485.
36 M. R.-R. I. Cruz-Cruz, M. A. Aguilar-Frutis, A. G. Rodriguez and R. López-Sandoval, *Synth. Met.*, 2010, **160**, 1501–1506.
37 E. S. Rania Gamal, N. Shash and M. G. El-Shaarawy, *Mater. Express*, 2014, **4**, 293–300.
38 R. Gamal, E. Sheha, N. Shash and M. El-Shaarawy, *Acta Phys. Pol., A*, 2015, **127**, 803–810.
39 Y. Zeng, L. Zhao, J. Zhang, Q. Li, D. Sun, Y. Ren, Y. Tang, G. Jin and H. Wang, *Small Sci.*, 2023, 2300017.
40 S. Ramesh, S.-C. Lu and E. Morris, *J. Taiwan Inst. Chem. Eng.*, 2012, **43**, 806–812.
41 C. R. Kumar, *Appl. Phys. A: Mater. Sci. Process.*, 2020, **126**, 148–156.
42 W. Zhang, F. Zhang, S. Liu, W. K. Pang, Z. Lin, Z. Guo and L. Chai, *Proc. Natl. Acad. Sci. U. S. A.*, 2023, **120**, e2219692120.
43 G. Leverick and Y. Shao-Horn, *Adv. Energy Mater.*, 2023, 2204094.
44 C. Z. Asim Khan, *Electrochem. Commun.*, 2014, **49**, 1–4.
45 R. Attias, M. Salama, B. Hirsch, Y. Goffer and D. Aurbach, *Joule*, 2019, **3**, 27–52.